Solution structure of an antimicrobial peptide buforin II

Gwan-Su Yi[a], Chan Bae Park[b], Sun Chang Kim[b], Chaejoon Cheong[a,*]

[a] *Magnetic Resonance Group, Korea Basic Science Institute, 52 Yeoeun-Dong, Yusung-Gu, Taejon 305-333, South Korea*
[b] *Department of Biological Sciences, Korea Advanced Institute of Science and Technology, Taejon 305-701, South Korea*

Received 23 July 1996; revised version received 1 October 1996

Abstract The structure of 21-residue antimicrobial peptide buforin II has been determined by using NMR spectroscopy and restrained molecular dynamics. Buforin II adopts a flexible random structure in H_2O. In trifluoroethanol (TFE)/H_2O (1 : 1, v/v) mixture, however, buforin II assumes a regular α-helix between residues Val[12] and Arg[20] and a distorted helical structure between residues Gly[7] and Pro[11]. The model structure obtained shows an amphipathic character in the region from Arg[5] to the C-terminus, Lys[21]. Like other known cationic antimicrobial peptides, the amphipathic structure might be the key factor for antimicrobial activity of buforin II.

Key words: Antimicrobial peptide; Buforin II; 2D-NMR; Molecular dynamics

1. Introduction

Recently, an antimicrobial peptide, buforin I, was isolated from the stomach tissue of an Asian toad, *Bufo bufo gargarizans*, and a more potent peptide buforin II was derived from buforin I [1]. These peptides show strong antimicrobial activities in vitro against a broad spectrum of microorganisms, including fungi [1]. Buforin II, a 21-residue cationic peptide containing the residues from Thr[16] to Lys[36] of buforin I, shows about two times higher activity than buforin I.

There have been comprehensive studies on a cationic antimicrobial peptide, magainin 2, isolated from the skin of *Xenopus laevis* [2]. Magainin 2 forms an α-helix in trifluoroethanol(TFE)/H_2O with charged residues on one side resulting in a large hydrophobic moment [3]. It interacts with bacterial and acidic model membranes [4] and destroys the ionic gradient across the cell membranes by forming ion channels [5]. For the buforin peptides, the structure and the detailed mechanism of the activity have not been resolved yet. Because the primary sequences of buforin II and magainin 2 are very different and the antimicrobial activities of buforin 2 are about 20 times higher than those of magainin 2, the structure of buforin II is of interest.

*Corresponding author. Fax: 82-42-865-3419.
E-mail: cheong@comp.kbsi.re.kr

Abbreviations: TFE, trifluoroethanol; DQF-COSY, double quantum filtered correlation spectroscopy; TOCSY, total correlation spectroscopy; NOESY, nuclear Overhauser enhancement spectroscopy; TPPI, time-proportional phase incrementation; RMD, restrained molecular dynamics; SA, simulated annealing; NOE(s), nuclear Overhauser effect(s)

2. Experimental

2.1. Peptide synthesis

Buforin II was synthesized by the Seoul Branch of the Korea Basic Science Institute (KBSI), using the solid-phase synthesis method on a Milligen 9050 Pepsynthesizer and fluoren-90-ylmethoxycarbony(Fmoc)-polypeptide active ester chemistry. The product was purified by reverse-phase HPLC on a Waters Delta-pak C18 column. The peptide was eluted with a H_2O/acetonitrile linear gradient containing 0.1% trifluoroacetic acid. The homogeneity was assessed by the reverse-phase HPLC on a Waters Delta-pak C18 column and by amino acid analysis on a Waters PICO-TAG® Amino Acid Analysis System. Its mass was confirmed on a Kratos MALDI-TOF spectrometer by the Mass Spectrometry Group at KBSI.

2.2. NMR spectroscopy

The NMR spectra were obtained on a Bruker DMX600 spectrometer. The samples were either in 50 mM phosphate buffer containing 10% D_2O at pH 7.0 or in TFE-d_3/50 mM phosphate buffer at pH 7.0 (1 : 1, by volume). The concentration of the peptide was about 2 mM and the experiments were performed at 10°C, 25°C and 35°C. Deuterated solvents were purchased from Aldrich and Cambridge Isotope Laboratory. For sequential assignments and structural determination, double quantum filtered correlation spectroscopy (DQF-COSY) [6], total correlation spectroscopy (TOCSY) [7] and nuclear Overhauser enhancement spectroscopy (NOESY) [8] experiments were performed. In TOCSY experiments, an MLEV-17 composite pulse sequence [9] was used for spin locking with a mixing time of 75 ms. The NOESY spectra were obtained with mixing times from 50 to 300 ms. Normally, the 2D data were acquired with 2 k (t_2 domain) ×512 (t_1 domain) data points, but for the DQF-COSY, 4 k×1 k data points were collected.

2.3. Structure calculation

Structures of buforin II were calculated using a molecular modeling program, NMRchitect (Biosym, Inc.) on an Indigo2 (Silicon Graphics, Inc.) workstation and a Cray Y-MP C916/16512 supercomputer in the System Engineering Research Institute (Taejon, Korea). Sixty-nine distance constraints for the structure calculations were obtained from the NOESY spectra acquired in TFE/H_2O at pH 7, 10°C. Volume integration was performed for NOESY mixing times of 50, 100, 150 and 250 ms and the crosspeak intensities were classified as strong, medium, or weak and converted into upper bounds of distance restraints of 2.8, 3.6 or 5.0 Å, respectively. The 12 $J_{HN\alpha}$ values were converted into loose dihedral angle restraints of $-30° < \phi < -100°$. Hydrogen bonding restraints were not used. Thirty initial structures were generated and refined using the distance geometry algorithm [10] DGII (Biosym, Inc.) with the NMR restraints.

The best structure which showed the lowest violation against the constraints was subjected to the restrained molecular dynamics (RMD) with the simulated annealing (SA) procedure [11] of NMRchitect (Biosym, Inc.). The consistent valence force field (CVFF) of DISCOVER 2.9 (Biosym, Inc.) was used for the molecular dynamics calculations. The SA procedure was started by restrained energy minimization which includes 100 iterations using the steepest descent minimization followed by 500 iterations using the conjugate gradients minimization. Then, 0.5 ps of RMD with 1 fs time steps was performed at 300 K followed by energy minimization. After this, the temperature was raised to 1000 K and the RMD was performed for 50 ps. Then, the temperature was gradually lowered to 300 K by 10 ps RMD in 5 steps. Finally, the steepest descent (100 iterations) and subsequent conjugate gradient minimizations (1500 iterations) were performed twice.

PII S0014-5793(96)01193-3

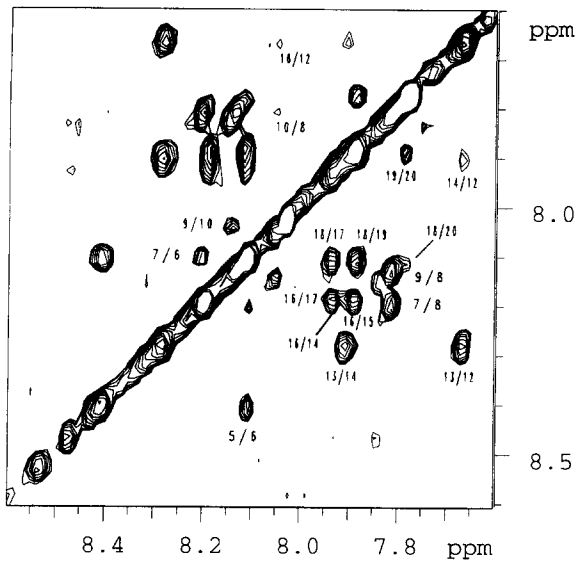

Fig. 1. NH/NH region of the NOESY spectrum of buforin II in TFE/H_2O (1 : 1, by volumes). The mixing time was 250 ms.

3. Results

The chemical shifts of buforin II have been assigned according to the standard assignment methods [12] using DQF-COSY, TOCSY and NOESY (Table 1).

Structural information of buforin II in TFE/H_2O was obtained from NOESY and DQF-COSY data. Fig. 1 shows the sequential NH(i)/NH(i+1) NOEs of buforin II in TFE/H_2O, which is a typical evidence of a helical conformation [12]. But, none of intense crosspeaks appears in the H_2O spectrum (data not shown). The sequential NH(i)/NH(i+1) NOEs appear in the region from Arg^5 to Arg^{20} (Figs. 1 and 2). Fig. 2 shows a summary of the NMR data acquired in TFE/H_2O. We find characteristic NOE connectivities indicative of helical structure in the region from Gly^7 to Arg^{20}. These connectivities include such as αH(i)/NH(i+3), αH(i)/NH(i+4), αH(i)/βH(i+3), βH(i)/NH(i+1) and NH(i)/NH(i+2) NOEs. The most dense region of NOE connectivities is between Pro^{11} and Leu^{18}. We conclude that the overall structure of the region from Gly^7 to Arg^{20} is helical with the most stable region ranging from Pro^{11} to Leu^{18}.

Although the overall conformation of the Gly^7–Arg^{20} segment is helical, there should be a distortion around Pro^{11} residue. The NOEs of δH(i)/NH(i+1) and βH(i)/NH(i+1) between Pro^{11} and Val^{12} are weak. In addition, the αH chemical shifts of Phe^{10} and Pro^{11} are not those of the standard α-helix [13,14]. The αH resonances normally shift upfield when the conformation changes from random coil to α-helix [13,14]. The αH chemical shifts of the C-terminal half region (Val^{12}–Lys^{21}) are shifted upfield as expected for α-helical geometry. However, the chemical shifts of Phe^{10} and Pro^{11} are shifted downfield. From the NOE connectivities and αH chemical shift data, we think that the backbone geometry near Pro^{11} is distorted into extended conformation.

This conformational distortion does not mean that the helix terminated at Pro^{11}. In the NOE and $J_{HN\alpha}$ analysis, the effects of Pro^{11} are not great. Some of the medium range connectivities indicative of the helical conformation such as NH(i)/NH(i+2), αH(i)/NH(i+3) and βH(i)/NH(i+1) NOEs extend over this region (Fig. 2). Therefore, we conclude that the changes in the chemical shifts near Pro^{11} are due to a local disturbance of the helix by the proline residue. This conclusion is not unique; there are several reports that α-helices can be extended over a proline residue [15,16]. Some reports suggest that the termination of the α-helical structure should depend on the interaction between the helical-end residue and the side chain groups of the neighboring residues [17,18].

From the NMR data, we conclude that the Gly^7–Arg^{20} segment is in a helical structure with a regular α-helix between Val^{12} and Arg^{20} and a distortion between Phe^{10} and Val^{12}. The smaller number of medium range connectivities in the Gly^7–Phe^{10} region shows that this region is more flexible than the C-terminal α-helix.

Based on the NMR data, we built a molecular model of buforin II in TFE/H_2O. Forty conformers were generated by SA starting from the DG structure. We selected eight conformers as the final converged structures; the others had higher conformational energy or too many constraint violations (Fig. 3). The distance violations for these eight conformers are less

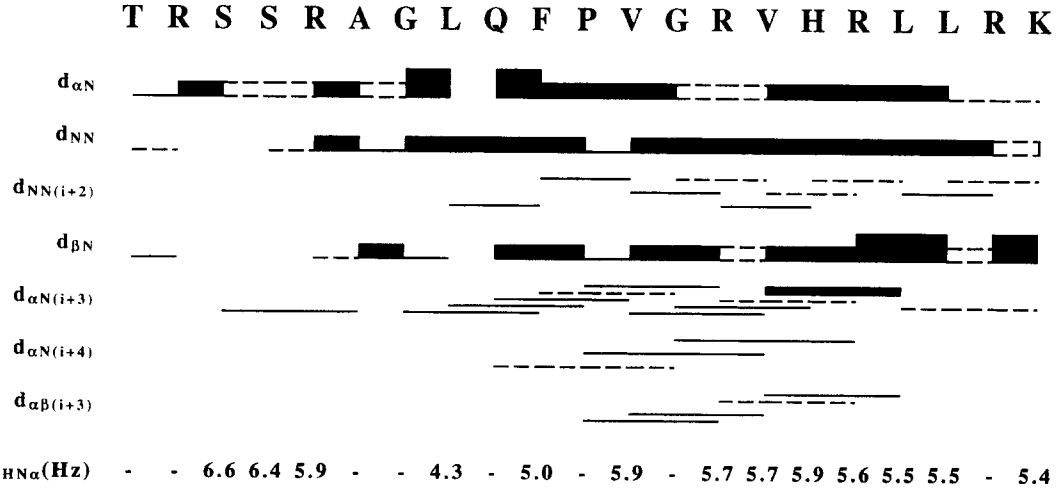

Fig. 2. Summary of the sequential and medium-range connectivities and some scalar coupling constants ($J_{HN\alpha}$) for buforin II in TFE/H_2O. The strength of the observed NOEs is represented by the thickness of bars. The dashed line or dashed box represents the NOEs from the overlapped crosspeaks. For the connectivities of Pro^{11}, the δH was used instead of the NH.

than 0.16 Å and their RMSDs are 2.28 Å for all atoms and 1.33 Å for the backbone atoms. As was expected from the NMR data, the conformers show a regular α-helix between Val^{12} and Arg^{20}. The distortion starts at Val^{12}. The average φ dihedral angle connecting Pro^{11} and Val^{12} is $-103 \pm 11°$ whereas that of a regular α-helix is −57°. The Gly^{7}–Val^{12} segment is composed of one and a half turns of helix. The diameter of this helix (~5.62 Å) is same as that of π-helix but its pitch (~6.82 Å) is larger than that of either a π-helix (4.73 Å) or an α-helix (5.4 Å).

4. Discussion

TFE is known to have a propensity to promote helix structure. But recent studies have shown that any peptide cannot become helical in TFE [19,20] and that it acts only within the context of a preexisting helix–coil equilibrium [21] rather than it creates a helix structure. This peptide does not exist as a single conformation even in 50% TFE. The $J_{HN\alpha}$ values (Fig. 2) represent averaged values of conformational ensembles. So, the structure that we present here should be regarded as one of the highly populated conformational states of buforin II in solution.

Because the sequence of buforin II is a part of the N-terminus of *Xenopus* histone H2A, the histone octamer structure, determined by X-ray crystallography [22], provides a good comparison. In the histone H2A structure, the region corresponding to the C-terminal half region (Val^{12} to Lys^{21}) and about five residues from the N-terminus of buforin II are α-helical [22]. The region corresponding to the C-terminal half region of buforin II is a part of the helix–loop–helix type structure element in histone octamer. Combined with our result, we conclude that the C-terminal region of buforin II retains the tendency to form an α-helix even in the amphiphilic environment. On the other hand, the N-terminal half of this peptide seems to have various structural possibilities depending on the environment. Noting that the C-terminal half region of buforin II is a part of DNA binding motif of histone H2A, it is possible that a direct buforin–DNA interaction might contribute to its antimicrobial activity.

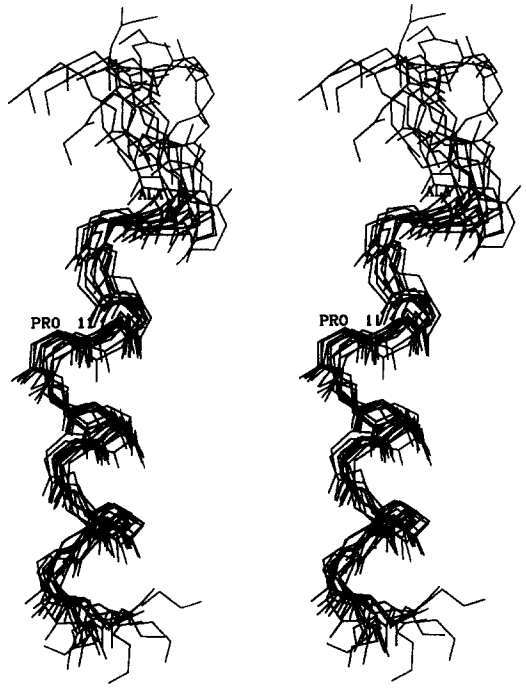

Fig. 3. Stereoview of the backbone atoms of the eight final structures of buforin II. The restraints for the structure calculations were obtained from the NMR data in TFE/H_2O at pH 7, 10°C.

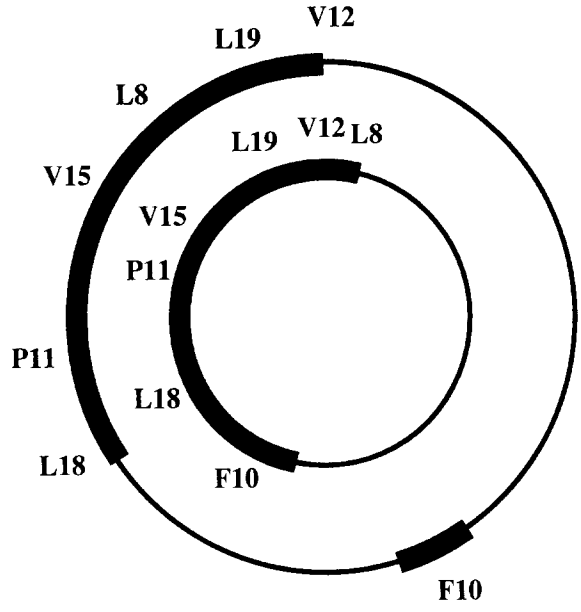

Fig. 4. The placement of hydrophobic residues of buforin II in a regular α-helix model (outer circle) and in the helical structure of our result (inner circle). The thick lines represent the hydrophobic region.

Table 1
NMR assignment of buforin II in H_2O/TFE (1 : 1, by volume) mixture

Residues	Chemical shift (ppm)[a]			
	HN	H^{α}	H^{β}	Others
Thr-1	8.16	4.30	4.45	H^{γ} 1.45
Arg-2	7.38	4.42	1.90, 1.98	H^{γ} 1.75; H^{δ} 3.25; NH 7.51, 6.72
Ser-3	8.52	4.51	3.89, 4.00	
Ser-4	8.41	4.51	3.93, 4.03	
Arg-5	8.40	4.36	1.85, 1.97	H^{γ} 1.69, 1.75; H^{δ} 3.21; NH 6.10, 7.39
Ala-6	8.10	4.30	1.47	
Gly-7	8.19	3.98		
Leu-8	7.81	4.35	1.73	H^{γ} 1.60; H^{δ} 0.91, 0.98
Gln-9	8.13	4.34	1.98, 2.09	H^{γ} 2.28, 2.33; NH 6.71, 7.37
Phe-10	8.05	4.89	3.09, 4.16	2,6H 7.29; 3.5H 7.34; 4H 6.707
Pro-11		4.53	2.07, 2.19	H^{γ} 1.99, 2.04; H^{δ} 3.45, 3.79
Val-12	7.68	3.86	2.06	H^{γ} 0.97, 1.04
Gly-13	8.29	3.98, 4.01		
Arg-14	7.91	4.21	1.93	H^{γ} 1.65, 1.76; H^{δ} 3.18; NH 7.29
Val-15	7.88	3.80	2.16	H^{γ} 0.94, 1.03
His-16	8.18	4.39	3.24	2H 8.03; 4H 7.08
Arg-17	7.93	4.19	1.97	H^{γ} 1.70, 1.77; H^{δ} 3.24; NH 7.43, 6.70
Leu-18	8.10	4.28	1.89	H^{γ} 1.68; H^{δ} 0.92 0.95
Leu-19	7.87	4.34	1.80	H^{γ} 1.56; H^{δ} 0.88
Arg-20	7.78	4.29	1.89, 1.96	H^{γ} 1.68; H^{δ} 3.21; NH 7.26
Lys-21	7.77	4.23	1.91	H^{γ} 1.47; H^{δ} 1.76; H^{ϵ} 3.04

[a]Chemical shifts were referenced to 3-(trimethylsilyl) propionic acid resonance. The estimated error was ±0.01 ppm.

As shown in the helical wheel diagram (Fig. 4), buforin II forms an amphipathic helical structure. For magainins [4,5] this geometry is considered the key factor for the formation of transmembrane pores, which will lead to cell death. In the regular α-helical geometry, amphipathic region of buforin II is limited to residues Pro^{11} to Lys^{21} (Fig. 4). The N-terminal half (Thr^{1} to Phe^{10}) cannot make an amphipathic alignment in the α-helical geometry. In our results, however, the amphipathic region is extended to the residues involving Arg^{5} through Lys^{21} due to the unusual helical conformation of Ala^{6}–Val^{12} segment.

Even though buforin II may interact with biological membranes like magainins, the mechanism of membrane interaction may be different. The length of the amphipathic region of buforin II (from Arg^{5} to Lys^{21}) is about 24 Å which is about two-thirds of magainin 2 (35 Å). Because the amphipathic region of buforin II cannot span the whole biological membrane (>30 Å for the hydrophobic region), the ion channel model suggested for magainin 2 [5] cannot be directly applied to buforin II. Further studies are needed to elucidate the antimicrobial activities of buforins.

Acknowledgements: We thank Dr. Dae-Sil Lee (KRIBB, Korea) and Professor Jung Hoon Shin (Inha Univ. Korea) for helpful discussions. This work was supported by grants (1995, 1996) from the Ministry of Science and Technology (MOST) (to C.C.) and by Research Center for New Biomaterials in Agriculture (1996) and the Ministry of Education (1996) (to S.C.K), the Republic of Korea.

References

[1] Park, C.B., Kim, M.S. and Kim, S.C. (1996) Biochem. Biophys. Res. commun. 218, 408–413.
[2] Erspamer, V. and Melchiorri, P. (1980) Trends Pharmacol. Sci. 1, 391–395.
[3] Marion, D., Zasloff, M. and Bax, A. (1988) FEBS Lett. 227, 21–26.
[4] Grant, E. Jr., Beeler, T.J., Taylor, K.M.P., Gable, K. and Roseman, M.A. (1992) Biochemistry 31, 9912–9918.
[5] Westerhoff, H.V., Juretic, D., Hendler, R.W. and Zasloff, M. (1989) Proc. Natl. Acad. Sci. USA 86, 6597–6601.
[6] Piantini, U., Sorensen, O.W. and Ernst, R.R. (1982) J. Am. Chem. Soc. 104, 6900–6801.
[7] Davis, D.G. and Bax, A.(1985) J. Am. Chem. Soc. 107, 2820–2823.
[8] Macura, S., Huang, Y., Suter, D. and Ernst, R.R. (1981) J. Magn. Reson. 43, 259–281.
[9] Bax, A. and Davis, D.G. (1985). J. Magn. Reson. 65, 355–360.
[10] Havel, T.F. (1991) Prog. Biophys. Mol. Biol. 56, 43–78.
[11] Nilges, M., Clore, G.M. and Gronenborn, A.M. (1988) FEBS Lett. 239, 129–136.
[12] Wüthrich, K. (1986) NMR of Proteins and Nucleic Acids, John Wiley, New York, 292 pp.
[13] Wishart, D.S., Sykes, B.D. and Richards, F.M. (1991) J. Mol. Biol. 222, 311–333.
[14] Merutka, G., Dyson, H.J. and Wright, P.E. (1995) J. Biomol. NMR 5, 14–24.
[15] Bruch, M.D. and Gierasch, L.M. (1990) J. Biol. Chem. 265, 3851–3858.
[16] Chi, S.-W., Yi, G.-S., Suh, J.-Y., Choi, B. and Kim, H. (1995) Biophys. J. 69, 2703–2709.
[17] Presta, L.G. and Rose, G.D. (1988) Science 240, 1632–1641.
[18] Richardson, J.S. and Richardson, D.C. (1988) Science 240, 1648–1652.
[19] Dyson, H.J., Merutka, G., Waltho, J.P., Lerner, R.A. and Wright, P.E. (1992) J. Mol. Biol. 226, 795–817.
[20] Dyson, H.J., Sayre, J.R., Merutka, G., Shin, H.C., Lerner, R.A. and Wright, P.E. (1992) J. Mol. Biol. 226, 819–835.
[21] Jasanoff, A. and Fersht, A.R. (1994) Biochemistry 33, 2129–2135.
[22] Arents, G., Burlingame, R.W., Wang, B.-C., Love, W.E. and Moudrianakis, E.N. (1991) Proc. Natl. Acad. Sci. USA 88, 10148–10152.